A Numerical Integration Method in Three Dimensional Complex Domain with Voronoi Polyhedra: Applications to First-Principles Electronic-Structure Calculations

Masaru AOKI

Ⅰ. Introduction

The development of general methods for three dimensional(3D) numerical integration effective for a complex domain is one of the most important and difficult problems in the numerical analysis. Increase of computer capability like recent parallel computers with large memory demands such kind of general and flexible scheme applicable to various fields like electronic-structure calculations, fluid dynamics, finite element method, boundary value problems, and electro-magnetic field calculations and so on. The main difficulties in the numerical integration are control of precision and treating of the complex domain of integration. A straightforward application of the standard cubature formula always needs a coordinate transformation dependent on the shape of the domain. In the case of an infinite domain like molecules or clusters, Becke's multicenter integration scheme[1)] is effective enough to keep accuracy for the charge of the system. Cellular methods associated with electronic structure calculations for molecules and solids have been developed by Boerrigter, Velde, and Baerends[2),3)] in which the space is partitioned into Wigner-Seitz (WS) cell (Voronoi polyhedron) constructed by planes that are perpendicular bisector planes of lines drawn from an atom to the surrounded atoms. Each WS cell is partitioned into the atomic sphere and the interstitial region. The integral inside the sphere is calculated with Gaussian quadrature in radial component and with product Gaussian formula in angular components. Gaussian

---

[1)] Becke, A.D., "A multicenter numerical integration scheme for polyatomic molecules", *J. Chem. Phys.* vol.88, 1988, pp.2547～2553.

[2)] Boerrigter, P.M., Velde, G.te, and Baerends, E.J., "Three-dimensional numerical integration for electronic structure calculations", *J. Int. J. Quantum Chem.* vol.33, 1988, pp.87～113.

[3)] Velde, G.te and Baerends, E.J., "Numerical integration for polyatomic systems", *J. Comput. Phys.* vol.99, 1992, pp.84～98.

quadrature is used to calculate the integral in the interstitial region with transformed three coordinates. Averill and Painter[4] improved the method by introducing the pseudospherical coordinates for general cone.

The author has developed a new integration method effective for a general 3D complex domain with sufficient accuracy on the basis of general Voronoi partition scheme. The essence of the method is an inclusion of concave Voronoi polyhedra, which allows us to treat complex domain of integration without coordinate transformation for the interstitial region. In the method, Voronoi partition is used not only in construction of the WS cells around each atom but also in partition of the interstitial regions to tetrahedra. The region is partitioned into convex Voronoi polyhedra and concave ones. The concave polyhedron is formed under situation that the polyhedron sticks on concave boundary surface. The Voronoi polyhedra can be further partitioned into tetrahedra and the integral of a function is calculated in each tetrahedron using standard cubature formula given by Stroud.[5]

This paper is organized as follows. In Chapter Ⅱ the integration scheme is presented. The algorithm of Voronoi partition is given in Chapter Ⅲ. In Chapter Ⅳ the precision of the numerical integration method is tested for the calculation of charge integral in simple cubic(s.c.), face centered cubic(f.c.c.), body centered cubic(b.c.c.), and diamond structures. In Chapter Ⅴ the method is applied to calculate the binding energy of Ar_2 dimer and the cohesive energy of Ar crystal. Summary and conclusions are in Chapter Ⅵ. Appendix A-C contain some additional notes of the Voronoi partition method.

Ⅱ. Integration Scheme

In numerical analysis the integral of a function $f(\vec{r})$ over a domain Ω,

$$I = \int_{\Omega} f(\vec{r}) d\vec{r}\,, \tag{1}$$

is approximately calculated by cubature formula with integration points $\vec{r}_k$ and appropriate weights ω_k as

$$I \cong Q(f) = \sum_k \omega_k f(\vec{r}_k). \tag{2}$$

In the present method, firstly random points for constructing Voronoi polyhedra are distributed in the domain. According to the geometrical configuration of the points, the domain is partitioned into Voronoi polyhedra and then each polyhedron is partitioned into tetrahedra. The integral over each tetrahedron is calculated with standard cubature formula based on a polynomial interpolation.[5] Then the integral (2) becomes

$$Q(f) = \sum_i \sum_j \omega_{tij}\, f(\vec{r}_{ij}) \;;\; i = 1,...,N_{tet},\;\; j = 1,...,N_g \tag{3}$$

where N_{tet} is the number of tetrahedra and N_g is the number of integration points in each

---

[4] Averill, F.W. and Painter, G.S., "Pseudospherical integration scheme for electronic-structure calculations", *Phys. Rev. B* vol.39, 1989, pp.8115～8121.

[5] Stroud, A.H., *Approximate Calculations of Multiple Integrals*, Prentice-Hall, Englewood Cliffs, NJ, 1971.

tetrahedron.

Ⅲ. Voronoi Partition

Generally, the shape of Voronoi polyhedron is convex in a bulk system such as crystals, glasses, and so on. Studies on the constructions of the Voronoi polyhedra have been confined to the convex polyhedron.[6),7)] However, the present method can treat the concave Voronoi polyhedron too. In the present paper, the domain of integration has a boundary which is composed of aggregation of polygons. If the boundary is curved surface, the surface is approximated with polygons which may include concave polygons. In partitioning the domain into Voronoi polyhedra, we obtain two types of polyhedra, i.e., concave polyhedra and convex polyhedra. The concave polyhedra are constructed on the concave boundary surface. The polyhedron is called *concave Voronoi polyhedron*. Figure 1 illustrates an example of the polyhedron. The concave part is the boundary of the domain. The algorithm of constructing general Voronoi polyhedra including the concave ones is presented in this chapter.

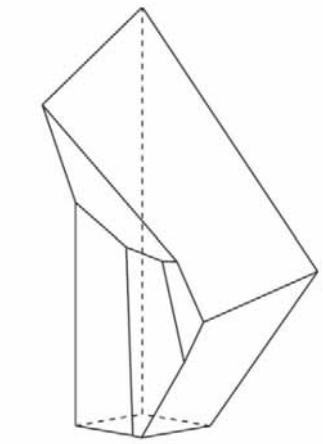

Fig.1. Figure of a concave Voronoi polyhedron.

1. Definitions

The domain of integration in 3D space is denoted by Ω. The shape of the domain is not restricted to convex. The boundary C of the domain is defined by the set of polygons $c_j \quad ; j = 1,..., N_c$,

$$C = \prod_{j=1}^{N_C} c_j, \tag{4}$$

where the vertices of the polygon c_j are sorted in a constant direction and $\vec{n}_j$ is the outward pointing normal vector. The shapes of the polygons are arbitrary. Hereafter, the polygon is

---

6) Finney, J.L., "A procedure for the construction of Voronoi polyhedra", *J. Comput. Phys*. vol.32, 1979, pp.137～143.

7) Tanemura, M., Ogawa, T. and Ogita, N., "A new algorithm for three- dimensional voronoi tessellation", *J. Comput. Phys.* vol.51, 1983, pp.191～207.

called *boundary polygon* (*boundary edge* in 2D case).

Points at coordinates $\vec{r}_1,\vec{r}_2,...,\vec{r}_{N_o} \in \Omega$ are denoted by symbols $o_1,o_2,...,o_{N_o}$. A function $f : o_i \to \Omega_i$ for $\Omega_i \subset \Omega$ such as the inverse $f^{-1} : \Omega_i \to o_i$ exists for the domain Ω. Then the domain Ω is partitioned into regions $\Omega_i ; i = 1,...,N_o$ for each o_i as

$$\Omega = \prod_{i=1}^{N_o} \Omega_i . \tag{5}$$

In this case the region Ω_i is a Voronoi polyhedron and the point o_i is the center for constructing the Voronoi polyhedron. The points $o_i ; i = 1,...,N_o$ is called *centers of Voronoi polyhedra* or *centers*. The set of the all centers is denoted by *O*. Then Voronoi polyhedron Ω_i is defined by

$$\Omega_i = \left\{ \; u \in \Omega \mid d(u,o_i) < d(u,o_j) \;\; ; \;\; j = 1,..., N_o (j \neq i) \; \right\} \tag{6}$$

where *u* is a point inside the domain Ω and $d(u,o_i)$ is Euclidean distance between the point *u* and the center o_i.

Furthermore, the Voronoi polyhedron Ω_i can be partitioned into Voronoi polyhedra $\Omega_{ij} ; j = 1,..., N_{oi}$, of which the centers are $o_{ij} ; j = 1,..., N_{oi}$, as

$$\Omega_i = \prod_{j=1}^{N_{oi}} \Omega_{ij} \tag{7}$$

Let us consider about the Voronoi polyhedron Ω_i. A set of the centers o_j around the center o_i is denoted by O_i, i.e., $O_i \equiv O - \{o_i\}$. Symmetry points $m_1, m_2, m_3,..., m_{N_c}$ of the center o_i exist with respect to boundary polygons $c_1, c_2, c_3,..., c_{N_c}$. The set of the m_j is denoted by M_i. A set Q_i is defined by $Q_i \equiv O_i \cup M_i$ and the elements of the set Q_i are denoted by $q_1, q_2, q_3,..., q_{N_q} ; N_q = (N_o - 1) + N_c$.

A perpendicular bisector plane of a segment $o_i q_j$ is denoted by $p(o_i, q_j)$ and the set by P_i. The elements of the set P_i are denoted by $p_1, p_2, p_3..., p_{N_q}$ too. Polygons $\sigma_1, \sigma_2, \sigma_3,..., \sigma_{N_\sigma}$ of the Voronoi polyhedron Ω_i are perpendicular bisector polygons of lines drawn from the o_i to the $q_j \in Q_i$. The edges of the Voronoi polyhedron Ω_i are denoted by $\gamma_1, \gamma_2, \gamma_3,..., \gamma_{N_\gamma}$.

An intersection of three planes $p(o_i,q_j)$, $p(o_i,q_k)$, $p(o_i,q_\ell) \in P_i$ is denoted by $t(j,k,\ell)$ and the set by T_i. The elements are denoted by $t_1, t_2, t_3,..., t_{N_t}$ too. Vertices $\lambda_1, \lambda_2, \lambda_3,..., \lambda_{N_\lambda}$ of the Voronoi polyhedron Ω_i are intersections of three planes $(\in P_i)$. The set of the vertices is denoted by Λ_i, i.e., $\Lambda_i \subset T_i$. The vertices on a polygon σ_j are denoted by

$\lambda_{j1},\lambda_{j2},\lambda_{j3},...,\lambda_{jN_{\lambda j}}$ and the set by Λ_{ij}.

The Voronoi polyhedron Ω_i can be partitioned into pyramids of which the bases are $\sigma_1,\sigma_2,\sigma_3,...,\sigma_{N_\sigma}$ and of which the top is o_i. The pyramids are denoted by $o_i\sigma_j; j=1,...,N_\sigma$. The each pyramid $o_i\sigma_j$ is further partitioned into tetrahedra of which the base is triangle $\lambda_{j1}\lambda_{jk+1}\lambda_{jk+2}; k=1,...,N_{\lambda j}-2$ and of which the top is o_i. The triangle is denoted by σ_{jk} and the tetrahedron is denoted by $o_i\sigma_{jk}$. The area of the σ_{jk} is denoted by $S(\sigma_{jk})$ and the volume of the $o_i\sigma_{jk}$ is denoted by $V(o_i\sigma_{jk})$. The area $S(\sigma_j)$ of the σ_j is given by

$$S(\sigma_j)=\sum_k S(\sigma_{jk}), \tag{8}$$

and the volume $V(o_i\sigma_j)$ of the $o_i\sigma_j$ is given by

$$V(o_i\sigma_j)=\sum_k V(o_i\sigma_{jk}). \tag{9}$$

The surface area $S(\Omega_i)$ of the Voronoi polyhedron Ω_i is given by

$$S(\Omega_i)=\sum_j S(\sigma_j), \tag{10}$$

and the volume $V(\Omega_i)$ of the Ω_i is given by

$$V(\Omega_i)=\sum_j V(o_i\sigma_j). \tag{11}$$

2. Voronoi Partition Algorithm

The Voronoi partition algorithm is shown as follows.

Step 1.

Distribute random points in a box which contains the domain Ω and select centers $o_i \in \Omega \;; i=1,...,N_o$. The selection method is presented in Appendix A. Add the $o_i \;; i=1,...,N_o$ to the set *O*.

Hereafter, we consider the algorithm to construct the Voronoi polyhedron Ω_i.

Step 2.

Find symmetry points m_j of o_i with respect to boundary polygon c_j. Add the $m_j \;; j=1,...,N_c$ to the set M_i and the set Q_i. The m_j in 2D case are shown as open circles in Fig.2.

Step 3.

Find centers o_j around the o_i. Add the $o_j \;; j=1,...,N_o-1$ to the set O_i and the set Q_i. The o_j in 2D case are shown as solid circles in Fig.2.

Step 4 and *5* are algorithms for all triplet $\alpha, \beta, \gamma \left(= 1, \ldots, N_q\right)$.

Step 4.

Calculate intersection $t_j = t\left(p_\alpha, p_\beta, p_\gamma\right)$ for $p_\alpha, p_\beta, p_\gamma \in P_i$.

Step 5.

Judge the $t_j \in \Lambda_j$ or $\notin \Lambda_j$ by using the three checks in Appendix B. If the $t_j \in \Lambda_j$, then add the t_j to the set $\Lambda_{j\alpha}$, the set $\Lambda_{j\beta}$, and the set $\Lambda_{j\gamma}$.

Following steps are algorithm to calculate the surface area $S\left(\Omega_i\right)$ and the volume $V\left(\Omega_i\right)$.

Step 6.

Sort the vertices $\lambda_{j1}, \lambda_{j2}, \lambda_{j3}, \ldots \in \Lambda_{ij};\ j = 1, \ldots, N_\sigma$ in a constant direction. We can sort the vertices based on the information for the polyhedron. That is, if $\lambda_1, \lambda_2 \in \Lambda_{ij}$ for $^\exists j$ and $\lambda_1, \lambda_2 \in \Lambda_{ik}$ for $^\exists k$, then $\lambda_1, \lambda_2 \in {}^\exists \gamma_\ell$.

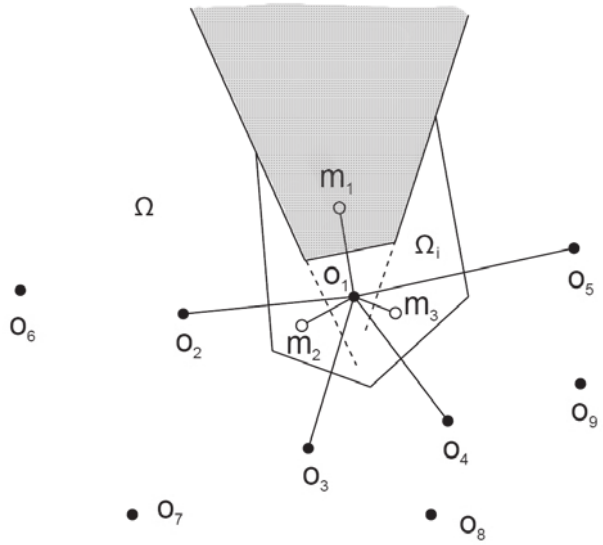

Fig.2. Cluster of points around the center o_1 in 2D case. Shaded region is the outside of the domain Ω.

Step 7.

Decompose the Voronoi polyhedron Ω_i into pyramids $o_i\sigma_j;\ j = 1, \ldots, N_\sigma$ and then into tetrahedra $o_i\sigma_{jk};\ j = 1, \ldots, N_\sigma, k = 1, \ldots, N_{\lambda j} - 2$ as shown in Fig.3.

Step 8.

Calculate surface area $S(\Omega_i)$ and volume $V(\Omega_i)$. From Eq.(8) and Eq.(10), the $S(\Omega_i)$ is given by

$$S(\Omega_i)=\sum_j\sum_k S(\sigma_{jk}) \;;\; j=1,\ldots,N_\sigma,\;\; k=1,\ldots,N_{\lambda j}-2, \tag{12}$$

and from Eq.(9) and Eq.(11), the $V(\Omega_i)$ is given by

$$V(\Omega_i)=\sum_j\sum_k V(o_i,\sigma_{jk}) \;;\; j=1,\ldots,N_\sigma,\;\; k=1,\ldots,N_{\lambda j}-2, \tag{13}$$

and

$$V(o_i,\sigma_{jk})=\frac{1}{3}V(\sigma_{jk})h_j, \tag{14}$$

where h_j is the height of the pyramid $o_i\sigma_j$. The $S(\sigma_{jk})$ and h_j are signed area and signed height respectively (see Appendix C).

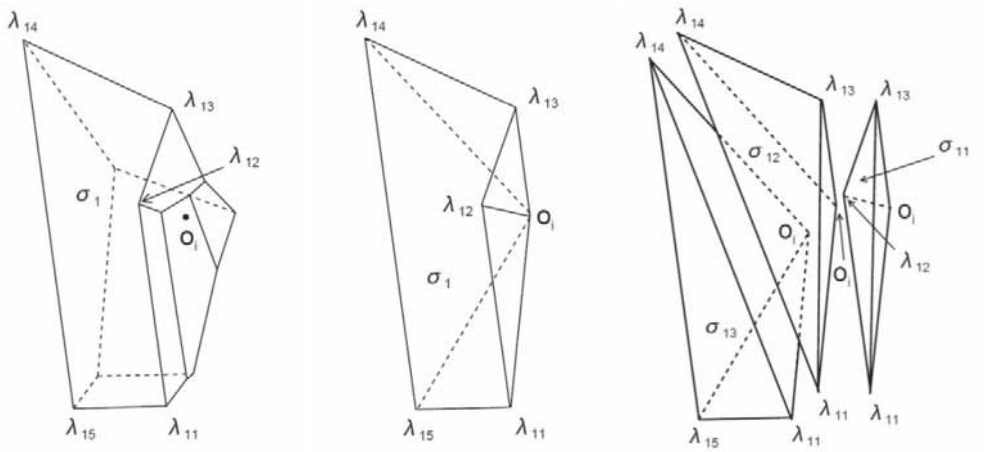

Fig.3. Partition process of a concave Voronoi polyhedron Ω_i shown in (a) into tetrahedra. The Voronoi polyhedron is decomposed to pyramids $o_i\sigma_i;\;\; j=1,\ldots,9$. One of the pyramids having the base σ_1 is shown in (b). The pyramid $o_i\sigma_1$ is further decomposed to tetrahedra $o_i\sigma_{11}$, $o_i\sigma_{12}$, and $o_i\sigma_{13}$ in (c), where the tetrahedra $o_i\sigma_{12}$ and $o_i\sigma_{13}$ have positive volume, but the tetrahedron $o_i\sigma_{11}$ has negative volume.

Ⅳ. Tests for precision of Numerical Integration Method

1. Integration Scheme inside WS Cell

Here, the method to calculate the integral of a function $f(\vec{r})$ in WS cell,

$$I = \int_{WS-cell} f(\vec{r})d\vec{r}\,, \tag{15}$$

is presented. Firstly, we separate the WS cell into two regions, i.e., the inside of atomic sphere and the interstitial region. Then the Eq.(15) becomes

$$I = I_s + I_i\,, \tag{16}$$

with

$$I_s = \int_{\substack{atomic\\ sphere}} f(\vec{r})d\vec{r}, \qquad I_i = \int_{\substack{interstitial\\ region}} f(\vec{r})d\vec{r}.$$

For cubic symmetry systems, the Eq.(16) becomes

$$I = I_s + 48I_i'\,, \tag{16}'$$

where

$$I_i' = \int_{1/48 interstitial\ region} f(\vec{r})d\vec{r}\,.$$

For tetragonal symmetry systems, the factor 48 changes to 24.

The integral I_s with radius r_a is given by

$$I_s = \int_0^a g(r)r^2 dr\,, \tag{17}$$

where

$$g(r) = \int_0^{2\pi}\int_0^{\pi} f(r,\theta,\phi)\sin\theta d\theta d\phi\,. \tag{18}$$

The Eq.(17) is calculated by a Gauss-Legendre integration formula.

$$I_s \cong Q(I_s) = \sum_i \omega_{ri}\, g(r_i) r_i^2 \quad ;i = 1,...,N_r\,, \tag{19}$$

where ω_{ri} is a weight of the coordinate r_i and N_r is the number of integration points. The function $g(r_i)$ in Eq.(18) is calculated by a product Gaussian formula[5] for each r_i as

$$g(r_i) \cong Q\{\ g(r_i)\ \} = \sum_j^{N_s} \omega_{sj}\, f(r_i,\theta_j,\phi_j)\,, \tag{20}$$

where ω_{sj} is a weight of the coordinate (θ_j,ϕ_j) on the sphere with radius r_i and N_s is the number of integration points.

The integral I_i' is calculated by the present method. That is, the interstitial region is partitioned into Voronoi polyhedra and then partitioned into tetrahedra by use of the method given in chapter Ⅲ. The integral of the function is calculated by a cubature formula. The domain of integration in chapter Ⅱ corresponds to the interstitial region and the integral of a function is calculated by Eq.(3).

2. Voronoi Partition of Interstitial Region

Figure 4(a) illustrates an example of partition of the interstitial region in the WS square cell. The region is enclosed with a circle and edges of the WS cell. The circle is approximated with a Voronoi polygon having the center *o*. The circle is called *atomic polygon* hereafter. The polygon is constructed by the edges that are perpendicular bisectors of lines drawn from the origin *o* to the points that are randomly distributed on a circle with twice radius of the original circle. The WS cell can be reduced to 1/8 wedge by symmetry operation. The interstitial region $u_1u_2u_3u_4$ is partitioned into twenty pieces of Voronoi polygon. The concave Voronoi polygons exist near the atomic polygon as shown in Fig.4(b) and convex ones exist in the rest region.

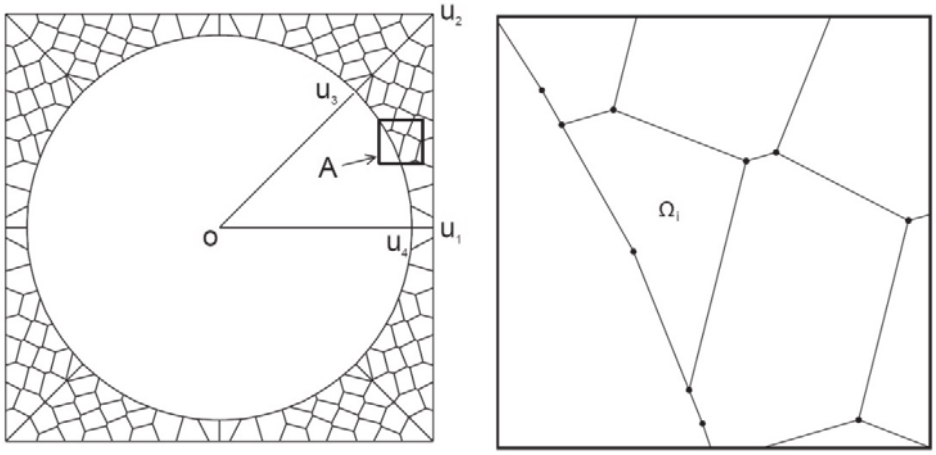

(a) (b)

Fig.4 (a) Voronoi partition of the interstitial region in the WS square cell. The circle *o* is approximated with Voronoi polygon of which the total number of boundary edges is 80. (b) Magnified figure of region *A* in (a). The Voronoi polygon Ω_i is concave one.

The construction procedure of the interstitial region in the s.c., f.c.c., b.c.c., and diamond structure is analogous to that of 2D case. The interstitial region is enclosed with an atomic sphere surface and planes of the WS cell. The concave polygons in 2D case correspond to concave polyhedra in 3D case. The atomic sphere is approximated with a Voronoi polyhedron. This polyhedron is called *atomic polyhedron*. The atomic polyhedron in the WS cell in f.c.c. structure is shown in Fig.5. The WS cell is reduced to 1/48 wedge by symmetry operation. The interstitial region of the 1/48 wedge is shown in Fig.6(a). The sphere surface is approximated with 11 pieces of polygon. The total number of boundary polygons becomes fifteen in this case. The 1/48 interstitial region is partitioned into two Voronoi polyhedra Ω_1 and Ω_2 as shown in Fig.6(b). In the case of non-uniform distribution of the centers, we distribute further points in each Voronoi polyhedron, of which the number is proportional to the volume of each Voronoi polyhedron, and partition into Voronoi polyhedra. Distributing three points in the Ω_2, we partition the Ω_2 into three Voronoi polyhedra in Fig.6(c).

The validity of the partition is checked by both the Euler's theorem and the sum of volumes of Voronoi polyhedra. The former theorem is given by $N_\lambda - N_\gamma + N_\sigma = 2$, where N_λ is the number of vertices, N_γ is the number of edges, and N_σ is the number of planes of each Voronoi polyhedron. All Voronoi polyhedra constructed in this study satisfy the theorem. The latter value is equal to the volume of the 1/48 interstitial region. The relative errors of the sum of the volumes in the four structures are less than 10^{-14}.

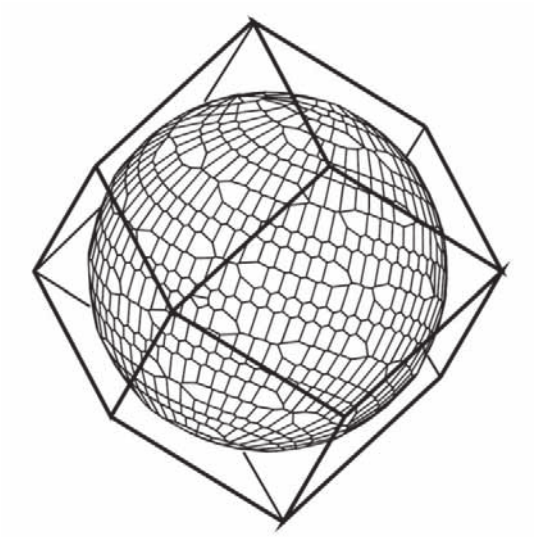

Fig.5. An atomic polyhedron in f.c.c. WS cell which is composed of thousand pieces of polygon.

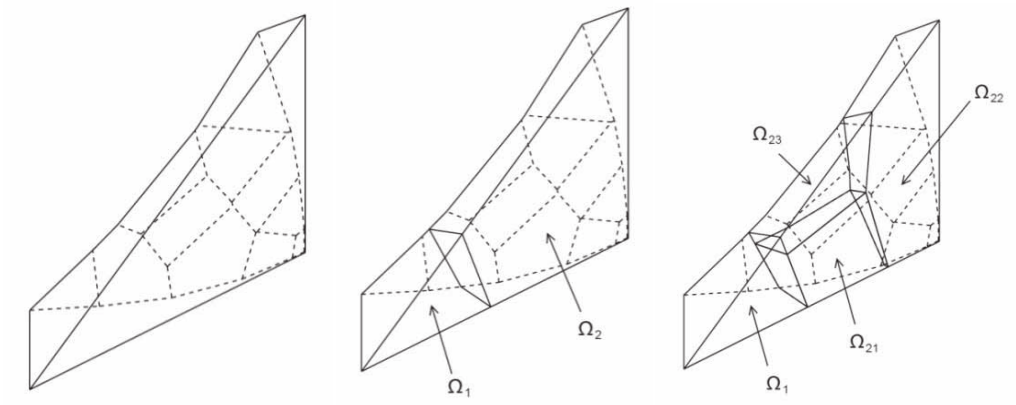

(a)　(b)　(c)

Fig.6 (a)The 1/48 interstitial region of f.c.c. WS cell in Fig.5. (b)Partition of the region in (a) into two Voronoi polyhedra Ω_1 and Ω_2. (c)Further partition of Voronoi polyhedron Ω_2 into three Voronoi polyhedra Ω_{21}, Ω_{22}, and Ω_{23}

3. Results of Integration

The electron charge density $\rho(\vec{r})$ is a basic integrand of electronic-structure calculations in order to estimate the accuracy of the present method. The $\rho(\vec{r})$ is given by superposition of charge density $\rho^{atom}(\vec{r})$ of a free atom,

$$\rho(\vec{r}) = \sum_i \rho^{atom}(\vec{r} - \vec{R}_i), \tag{21}$$

where $\vec{R}_i$ is the position of nuclei. The charge density $\rho^{atom}(\vec{r})$ is expressed by linear combination of Yukawa type functions[8] as

$$\rho^{atom}(\vec{r}) = \frac{Z}{4\pi r} \sum_{j=1}^{3} A_j \alpha_j^2 exp(-\alpha_j r), \tag{22}$$

where Z is the nuclear charge and the parameters A_j, α_j are given by Salvat, F *et al*.[8] The exact charge integral value in the WS cell is Z. We choose Po(Z=84) as s.c., Cu(Z=29) as f.c.c., W(Z=74) as b.c.c., and Si(Z=14) as diamond structure. The exact charge integral value in the interstitial region are 0.9314824307 in s.c., 0.4502970484 in f.c.c., 1.233486671 in b.c.c., and 1.470762851 in diamond structure.

The relative errors of the charge integral value in the interstitial region are shown in Table I(a)-(d) together with the number of integration points. A single number in the second column in Table I indicates that the reduced interstitial region consists of one concave Voronoi polyhedron itself. The accuracy of approximating of the sphere surface depends on the number of the boundary polygons. The number of integration points is fifteen times of the number of tetrahedra and depends on two factors: the number of boundary polygons and the number of Voronoi polyhedra. Therefore it is necessary to increase both numbers for high precision calculation.

In s.c. structure shown in Table I(a), the errors decrease approximately with increasing the number of the integration points. The relative errors of the charge in the interstitial region are less than 10^{-4}. Then the relative errors of the total charge is less than 10^{-6}. Thus the accuracy of the charge integral value is sufficient to calculate the cohesive energy based on the density functional theory. In the other structures shown in Table I(b), (c), and (d), the overall features are the same as those of the s.c. structure. Consequently, the present method is proved to be applicable to the charge integral in high precision without depending on the shape of domain.

---

[8] Salvat, F., Martinez, J.D., Mayol, R. and Parellada, J., "Analytical Dirac-Hartree- Fock-Slater screening function for atoms (Z=1–92)", *Phys. Rev. A* vol.36, 1987, pp.467～474.

Table I. The relative errors and the total charges calculated by the present method for (a)s.c.(Po, Z=84), (b)f.c.c.(Cu, Z=29), (c)b.c.c.(W, Z=74), and (d)diamond (Si, Z=14) structures as a function of the numbers of boundary polygons, Voronoi polyhedra, tetrahedra, and integration points. The number of integration points is fifteen times the number of tetrahedra. The exact charge integral values in the interstitial region are 0.9314824307 for s.c., 0.4502970484 for f.c.c., 1.233486671 for b.c.c., and 1.470762851 for diamond structure.

(a)

Number of boundary polygons	Number of Voronoi polyhedra	Number of tetrahedra	Number of integration points	Charge in interstitial region	Relative error	Total charge
6	1	12	180	0.9822443	5.45E-2	84.050761821
6	2	24	360	0.9823663	5.46E-2	84.050883840
6	3	36	540	0.9823628	5.46E-2	84.050880359
6	4	52	780	0.9823592	5.46E-2	84.050876778
6	6	80	1200	0.9823746	5.46E-2	84.050892155
15	1	48	720	0.9333946	2.05E-3	84.001912134
15	2	72	1080	0.9334935	2.16E-3	84.002011023
15	3	88	1320	0.9335003	2.17E-3	84.002017855
15	4	100	1500	0.9334936	2.16E-3	84.002011172
15	6	132	1980	0.9335206	2.19E-3	84.002038198
25	1	88	1320	0.9320878	6.50E-4	84.000605401
25	2	112	1680	0.9321957	7.66E-4	84.000713225
25	3	128	1920	0.9321990	7.69E-4	84.000716514
25	4	144	2160	0.9321925	7.62E-4	84.000710092
25	6	180	2700	0.9322193	7.91E-4	84.000736834
35	1	128	1920	0.9312034	3.00E-4	83.999720914
35	2	164	2460	0.9313088	1.86E-4	83.999826373
35	3	180	2700	0.9313171	1.78E-4	83.999834640
35	4	196	2940	0.9313086	1.87E-4	83.999826183
35	6	236	3540	0.9313385	1.54E-4	83.999856108
45	1	168	2520	0.9313328	1.61E-4	83.999850378
45	2	212	3180	0.9314388	4.68E-5	83.999956375
45	3	228	3420	0.9314475	3.75E-5	83.999965089
45	4	244	3660	0.9314388	4.68E-5	83.999956383
45	6	284	4260	0.9314690	1.45E-5	83.999986532
55	1	208	3120	0.9313318	1.62E-4	83.999849403
55	2	260	3900	0.9314377	4.80E-5	83.999955293
55	3	276	4140	0.9314461	3.90E-5	83.999963672
55	4	292	4380	0.9314374	4.83E-5	83.999954981
55	6	336	5040	0.9314675	1.60E-5	83.999985105

(b)

Number of boundary polygons	Number of Voronoi polyhedra	Number of tetrahedra	Number of integration points	Charge in interstitial region	Relative error	Total charge
6	1	12	180	0.4560236	1.27E-2	29.005726528
6	2	28	420	0.4560326	1.27E-2	29.005735595
6	3	44	660	0.4560341	1.27E-2	29.005737012
6	4	60	900	0.4560320	1.27E-2	29.005734925
6	6	96	1440	0.4560335	1.27E-2	29.005736453
15	1	48	720	0.4501929	2.31E-4	28.999895866
15	2	76	1140	0.4501943	2.28E-4	28.999897210
15	3	96	1440	0.4502044	2.06E-4	28.999907376
15	4	124	1860	0.4502054	2.04E-4	28.999908360
15	6	156	2340	0.4502055	2.03E-4	28.999908429
25	1	88	1320	0.4504911	4.31E-4	29.000194065
25	2	120	1800	0.4504963	4.43E-4	29.000199297
25	3	144	2160	0.4505064	4.65E-4	29.000209304
25	4	172	2580	0.4505075	4.67E-4	29.000210429
25	6	224	3360	0.4505076	4.68E-4	29.000210569
35	1	128	1920	0.4503895	2.05E-4	29.000092457
35	2	148	2220	0.4504047	2.39E-4	29.000107615
35	3	156	2340	0.4504048	2.39E-4	29.000107749
35	4	192	2880	0.4504042	2.38E-4	29.000107186
35	6	248	3720	0.4504045	2.39E-4	29.000107491
45	1	168	2520	0.4502851	2.65E-5	28.999988054
45	2	192	2880	0.4502996	5.66E-6	29.000002550
45	3	200	3000	0.4502998	6.01E-6	29.000002708
45	4	236	3540	0.4502990	4.41E-6	29.000001985
45	6	296	4440	0.4502993	5.10E-6	29.000002298
55	1	208	3120	0.4502866	2.33E-5	28.999989515
55	2	236	3540	0.4503011	8.89E-6	29.000004005
55	3	244	3660	0.4503012	9.25E-6	29.000004165
55	4	288	4320	0.4503005	7.67E-6	29.000003456
55	6	356	5340	0.4503008	8.39E-6	29.000003777

(c)

Number of boundary polygons	Number of Voronoi polyhedra	Number of tetrahedra	Number of integration points	Charge in interstitial region	Relative error	Total charge
7	1	16	240	1.2357386	1.83E-3	74.002251961
7	2	32	480	1.2357292	1.82E-3	74.002242536
7	3	52	780	1.2357332	1.82E-3	74.002246496
7	4	68	1020	1.2357315	1.82E-3	74.002244779
7	6	112	1680	1.2357325	1.82E-3	74.002245875
16	1	52	780	1.2338407	2.87E-4	74.000354007
16	2	72	1080	1.2338208	2.71E-4	74.000334085
16	3	108	1620	1.2338244	2.74E-4	74.000337684
16	4	112	1680	1.2338242	2.74E-4	74.000337577
16	6	156	2340	1.2338246	2.74E-4	74.000337907
26	1	92	1380	1.2332842	1.64E-4	73.999797546
26	2	120	1800	1.2332625	1.82E-4	73.999775830
26	3	156	2340	1.2332660	1.79E-4	73.999779326
26	4	168	2520	1.2332661	1.79E-4	73.999779427
26	6	216	3240	1.2332663	1.79E-4	73.999779671
36	1	132	1980	1.2335219	2.86E-5	74.000035264
36	2	168	2520	1.2335001	1.09E-5	74.000013453
36	3	208	3120	1.2335036	1.37E-5	74.000016919
36	4	224	3360	1.2335036	1.37E-5	74.000016883
36	6	276	4140	1.2335038	1.39E-5	74.000017141
46	1	172	2580	1.2335246	3.08E-5	74.000037935
46	2	216	3240	1.2335009	1.16E-5	74.000014259
46	3	260	3900	1.2335044	1.44E-5	74.000017710
46	4	276	4140	1.2335043	1.43E-5	74.000017639
46	6	336	5040	1.2335046	1.45E-5	74.000017894
56	1	212	3180	1.2335103	1.92E-5	74.000023658
56	2	264	3960	1.2334867	1.16E-8	73.999999986
56	3	312	4680	1.2334901	2.79E-6	74.000003441
56	4	340	5100	1.2334901	2.79E-6	74.000003439
56	6	400	6000	1.2334904	2.99E-6	74.000003693

(d)

Number of boundary polygons	Number of Voronoi polyhedra	Number of tetrahedra	Number of integration points	Charge in interstitial region	Relative error	Total charge
7	1	16	240	1.4770469	4.27E-3	14.006284061
7	2	28	420	1.4770800	4.30E-3	14.006317175
7	3	56	840	1.4771201	4.32E-3	14.006357244
7	5	84	1260	1.4771307	4.33E-3	14.006367864
7	6	100	1500	1.4771337	4.33E-3	14.006370800
16	1	52	780	1.4723688	1.09E-3	14.001605936
16	2	80	1200	1.4725326	1.20E-3	14.001769736
16	3	100	1500	1.4724677	1.16E-3	14.001704803
16	4	116	1740	1.4725252	1.20E-3	14.001762336
16	6	156	2340	1.4725049	1.18E-3	14.001742071
26	1	92	1380	1.4715007	5.02E-4	14.000737873
26	2	104	1560	1.4716157	5.80E-4	14.000852836
26	3	140	2100	1.4715988	5.68E-4	14.000835989
26	4	172	2580	1.4716668	6.15E-4	14.000903975
26	6	200	3000	1.4716261	5.87E-4	14.000863265
36	1	132	1980	1.4703757	2.63E-4	13.999612885
36	2	144	2160	1.4704716	1.98E-4	13.999708791
36	3	184	2760	1.4704494	2.13E-4	13.999686515
36	4	220	3300	1.4705294	1.59E-4	13.999766532
36	6	244	3660	1.4704827	1.90E-4	13.999719861
46	1	172	2580	1.4700441	4.89E-4	13.999281263
46	2	184	2760	1.4701402	4.23E-4	13.999377358
46	3	224	3360	1.4701168	4.39E-4	13.999353947
46	4	276	4140	1.4701970	3.85E-4	13.999434132
46	6	296	4440	1.4701505	4.16E-4	13.999387620
56	1	212	3180	1.4707413	1.46E-5	13.999978472
56	2	244	3660	1.4706876	5.12E-5	13.999924750
56	3	288	4320	1.4707023	4.12E-5	13.999939408
56	4	268	4020	1.4707277	2.39E-5	13.999964806
56	6	308	4620	1.4707293	2.28E-5	13.999966406

Ⅴ. Applications to First-Principles Electronic-Structure Calculations

We calculate the cohesive energy of Ar crystal and the binding energies of Ar_2 dimer based on the density functional theory of the Thomas-Fermi-Dirac-Weizsäcker model[9] to evaluate the present numerical integration method.

1. Energy Density Functionals

In the density functional theory of the Thomas-Fermi-Dirac-Weizsäcker model, the total energy of the system is given by

$$E_{tot} = E_{kin}[\rho] + E_{ee}[\rho] + E_{eN}[\rho] + E_x[\rho] + E_{NN}, \tag{23}$$

where electron-electron electrostatic energy $E_{ee}[\rho]$, electron-nucleus electrostatic energy $E_{eN}[\rho]$, and nucleus-nucleus electrostatic energy E_{NN} are given by

$$E_{ee}[\rho] = \frac{1}{2}\int V_e(\vec{r})\rho(\vec{r})d\vec{r}, \tag{24}$$

$$E_{eN}[\rho] = \frac{1}{2}\int V_N(\vec{r})\rho(\vec{r})d\vec{r}, \tag{25}$$

$$E_{NN} = \frac{1}{2}\sum_{i\neq j}\sum \frac{Z_{Ri}Z_{Rj}}{\left|\vec{R}_i - \vec{R}_j\right|}, \tag{26}$$

where $V_e(\vec{r})$ is electrostatic potential of electrons and $V_N(\vec{r})$ is electrostatic potential of nuclei. The integrals are calculated over all space in the dimer system and over WS cell in crystalline system. The Kinetic energy $E_{kin}[\rho]$ and the exchange energy $E_x[\rho]$ are given by

$$E_{kin} = C_k\int\rho(\vec{r})^{5/3}d\vec{r} + \frac{1}{72}\int\frac{\left|\nabla\rho(\vec{r})\right|^2}{\rho(\vec{r})}d\vec{r}, \qquad C_k = \frac{3}{10}(3\pi)^{2/3}, \tag{27}$$

$$E_x = C_e\int\rho(\vec{r})^{4/3}d\vec{r}, \qquad C_e = -\frac{3}{4}\left(\frac{3}{\pi}\right)^{1/3}, \tag{28}$$

where second term in Eq.(27) is Weizsäcker term. The charge density $\rho(\vec{r})$ is given by Eq.(21). The atomic electrostatic potential[8] is given by

$$V_{eN}^{atom}(\vec{r}) = -\frac{Z}{r} + \int\frac{\rho_{(\vec{r}')}}{\left|\vec{r}-\vec{r}'\right|}d\vec{r}' = -\frac{Z}{r}\sum_{j=1}^{3}A_j exp(-\alpha_j r). \tag{29}$$

The electrostatic energy is calculated as follows.

$$E_{ee}[\rho] + E_{eN}[\rho] + E_{NN} = \frac{1}{2}\sum_i\int V_{eN}^{atom}(\vec{r}' - \vec{R}_i)\rho(\vec{r}')d\vec{r}' - \frac{1}{2}\left[\sum_i{}' V_{eN}^{atom}(\vec{R}_i) + V_e^{atom}(0)\right]Z, \tag{30}$$

where the Σ' indicates the exclusion of the vector $\vec{R}_1 = (0,0,0)$. The $V_e^{atom}(0)$ is given by

---

[9] Kryachko, E.S. and Ludena, E.V., *Energy Density Functional Theory of Many-Electron Systems*, Kluwer Academic Publishers, 1990.

$$V_e^{atom}(0) = Z\sum_{i=1}^{3} A_i\alpha_i \,. \tag{31}$$

The cohesive(or binding) energy ΔE per atom is calculated by

$$\Delta E = \frac{1}{N_a} E_{tot} - E_{tot}^{atom}, \tag{32}$$

where N_a is the number of atoms in the system and E_{tot}^{atom} is the total energy of an isolated atom.

2. Cohesive Energy Calculation

The cohesive energy of Ar crystal(f.c.c. structure) is calculated by using the integration points and weights which are examined carefully in Table I(b). The number of integration points in the 1/48 interstitial region is 2,880. The cohesive energy of Ar crystal is shown in Fig.7. The cohesive energy is converged within a tolerance of 10^{-4}. The lattice constant given by the present method is 8.85 a.u.. The experimental lattice constant[10] is 10.0 a.u.. The difference of the lattice constant from the experimental value[10)] is slightly 1.15 a.u.. Therefore the present numerical integration method is applicable to calculate the cohesive energy of Ar crystal.

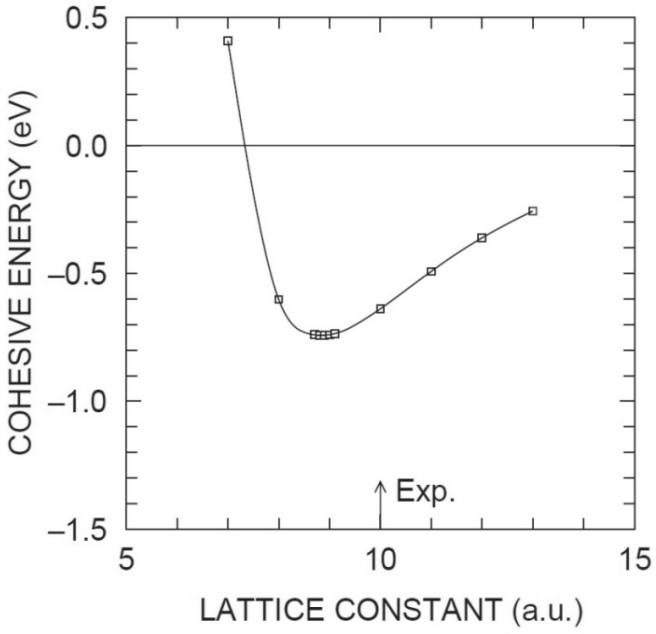

Fig.7. Cohesive energy of Ar crystal as a function of lattice constant. The experimental lattice constant[10] (Exp.) is 10.0 a.u..

[10)] Kittel, C., *Introduction to Solid State Physics*, 6th edition, John Wiley & Sons. New York, 1986.

3. Binding Energy Calculation

The atomic positions of Ar_2 dimer are arranged as shown in Fig.8(a). The space is partitioned into three region. The region I is inside an atomic sphere with radius r_1, the region III is outside a sphere with radius r_2, and the region II is the rest region. We calculate the integral of the functions over the regions I and III by Gaussian quadrature and product Gaussian formula. On the other hand, The presented method is used to calculate the integral over the region II. In partitioning the region II into Voronoi polyhedra, we use the 1/48 reduced region although figure 8(b) illustrates the 1/16 reduced region. The binding energy of Ar_2 dimer is shown in Fig.9. The number of integration points in the 1/48 region II increases corresponding to the interatomic distance. For example, the maximum and the minimum numbers of points are 30,240 and 27,480 respectively.

The equilibrium interatomic distance calculated by the present method is 6.15 a.u.. The difference of the equilibrium interatomic distance to experimental value[11] is slightly 0.95 a.u.. Therefore the present numerical integration method is applicable to calculate the binding energy of Ar_2 dimer.

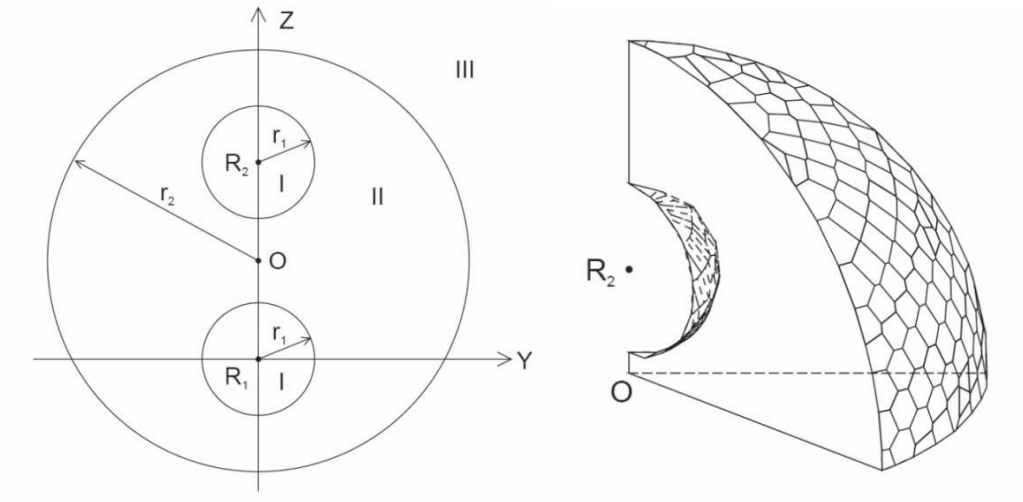

(a)　　(b)

Fig.8 (a)Projected figure of the domain of integration to *Y-Z* plane. The two Ar atoms, of which the interatomic distance is *d*, are positioned at $\vec{R}_1 = (0,0,0)$ and $\vec{R}_2 = (0,0,d)$. The radii r_1 and r_2 are 2 and 8 a.u. respectively. (b)The 1/16 reduced region II. The 1/8 inside sphere surface is approximated with 51 pieces of polygon and the 1/16 outside sphere surface is approximated with 100 pieces of polygon.

[11] Huber, K.P. and Herzberg, G., *Molecular Spectra and Molecular structure IV constants of diatomic molecules*, Van Nostrand Reinhold Company Inc., 1979.

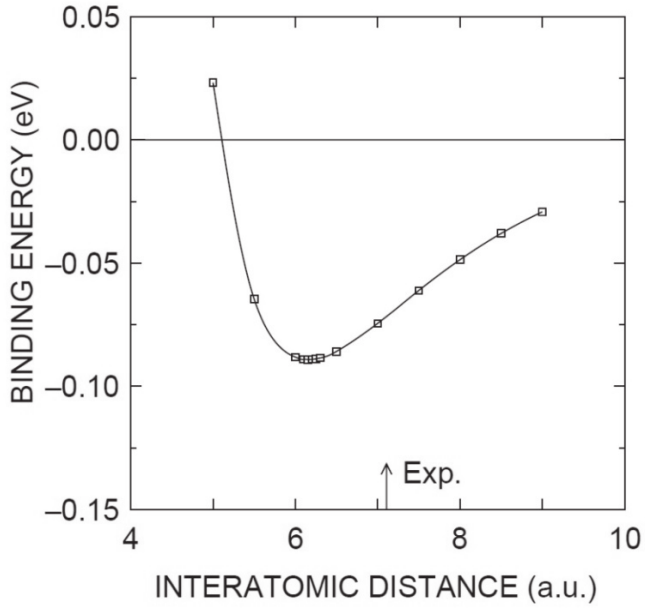

Fig.9. Binding energy of Ar_2 dimer as a function of interatomic distance. The experimental equilibrium interatomic distance[11] (Exp.) is 7.10 a.u..

Ⅵ. Summary and Conclusions

The author has developed a new numerical integration method in 3D complex domain based on the Voronoi partitions without a coordinate transformation adapted to the shape of the domain. In the method, the domain, of which the boundary surface is approximated with polygons, is partitioned into Voronoi polyhedra corresponding to randomly distributed points. Each Voronoi polyhedron is further partitioned into tetrahedra so as to be applicable to the calculation of the integral. Introduction of concave Voronoi polyhedra frees us from intractable restrictions of the complex domain of integration.

In order to evaluate the present method, we have investigated the two things. Firstly, we have investigated whether or not the present method is effective to the charge integrations in various structures. Then the relative errors have been less than 10^{-6}. Thus the present method is proved to be applicable to the charge integration in high precision without depending on the shape of the domain. Secondly, we have applied the method to cohesive energy calculations based on density functional theory. Then we have found that the method is applicable to calculate both the cohesive energy of Ar crystal and the binding energy of Ar_2 dimer. Consequently, the present method has been proved to be effective for the first-principles electronic-structure calculation.

Appendix A: Selection Method of Points inside Domain

Here, the selection method of the points existing inside a domain is presented. We assume the boundary C consists of edges in 2D case and consists of polygons in 3D case. We also assume that no point exists on boundary edge in 2D case (boundary polygon in 3D case).

A1. The Case of 2D Domain

As shown in Fig.10, we position the origin of the system on the coordinate r_ℓ and draw a line from the point to x-direction. The line intersects with a boundary edge c_k : $(x_{ck}, y_{ck})-(x_{ck+1}, y_{ck+1})$ at the intersection $\xi_k : (x_{\xi k}, y_{\xi k})$. Then the coordinate of ξ_k is given by

$$x_{\xi k} = \frac{x_{ck+1} - x_{ck}}{y_{ck+1} - y_{ck}} y_{ck} + x_{ck}, \qquad y_{\xi k} = 0 . \tag{A.1}$$

The coordinates of the intersection are calculated about all boundary edges. The case of $y_{ck+1} - y_{ck} = 0$ corresponds to not existing of the intersection. By counting the number of ξ_k that satisfies both the condition $x_{\xi k} \geq 0$ and $y_{ck+1} y_{ck} < 0$, we can distinguish whether the point exists inside the domain or not. That is, if the number is even, then the point is outside the domain Ω. Conversely, if the number is odd, the point is inside the domain Ω.

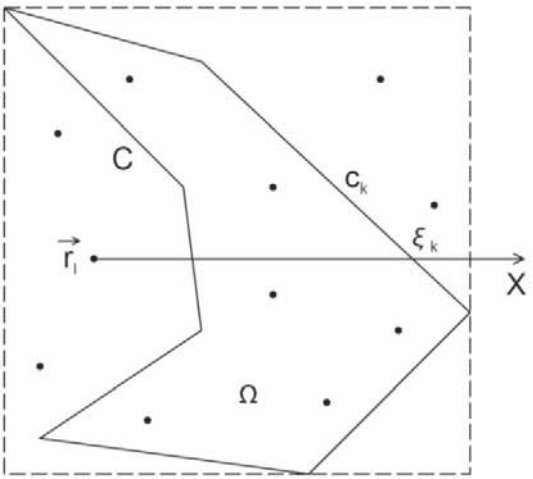

Fig.10. Schematic representation of the distribution of random points inside a 2D box shown by the broken line. The solid line represents the boundary C.

A2. The Case of 3D Domain

The basic idea is the same as the 2D case. We position the origin of the system at the coordinate r_ℓ. The coordinates of the vertices of each boundary polygon c_j are denoted by (x_{jk}, y_{jk}, z_{jk}) ; $j = 1,...,N_c$, $k = 1,...,N_j$ and the component of normal vector $\vec{n}_j$ of the c_j is denoted by (n_{xj}, n_{yj}, n_{zj}). The coordinates $(x_{\xi j}, y_{\xi j}, z_{\xi j})$ of the intersection ξ_j between each polygon c_j and a line from the point r_ℓ to x-direction are given by

$$x_{\xi j} = \frac{n_{xj}x_{jl} + n_{yj}y_{jl} + n_{zj}z_{jl}}{n_{xj}}, \qquad y_{\xi j} = z_{\xi j} = 0 . \tag{A.2}$$

The case of $n_{xj} = 0$ corresponds to not existing of the intersection. By counting the number of ξ_j that satisfies both the condition $x_{\xi j} \geq 0$ and $\xi_j \in c_j$, we can distinguish whether the point exists inside the domain or not. That is, if the number is even, then the point is outside the domain Ω. Conversely, if the number is odd, the point is inside the domain Ω.

Appendix B: Selection Method of Vertices of Voronoi Polyhedron

Selection method of the vertices $\lambda_1, \lambda_2, \lambda_3, ..., \lambda_{N\lambda}$ of the (concave) Voronoi polyhedron Ω_i is shown by using the example in 2D case as shown in Fig.11. If an intersection of three planes passes through the following three checks, then the intersection is accepted as the vertex of the Voronoi polyhedron Ω_i.

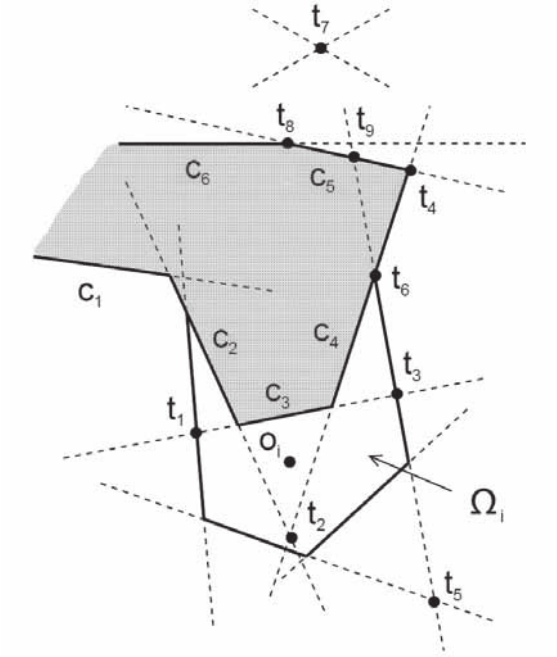

Fig.11. An example of intersections around the center o_i in 2D case. Shaded region is the outside of the domain Ω.

Consider an intersection $t_\alpha = t(p_j, p_k, p_\ell)$ for planes $p_j, p_k, p_\ell \in P_i$.

Check 1.

When $^{\exists} c_\beta \subset \{p_j, p_k, p_\ell\}$, if $t_\alpha \in c_\beta$, then the t_α passes this check. For instance, the intersection t_1 does not pass this check, since the intersection is outside the boundary edge c_3. The intersections t_2 and t_3 also do not pass this check.

Check 2.

If an intersection t_α is located outside an perpendicular bisector plane p_j which do not include $^{\exists}c_\alpha$, the t_α does not pass this check. For instance, the intersections t_4 and t_5 also do not pass this check.

Check 3.

When $t_\alpha \notin {}^{\exists}c_\beta$, if $^{\exists}c_\beta$ exists between o_i and t_α, i.e., the segment $o_i t_\alpha \cap c_\beta \neq \varnothing$, then the t_α does not pass this check. For instance, t_6 passes this check. However t_7 does not pass this check because there are c_3 and c_5 as the c_β. Here, we must pay attention to points such as t_8 and t_9. Although the intersections t_8 and t_9 are not vertices of the concave Voronoi polyhedron Ω_i, the intersections pass the three checks and accepted as the vertices. However the existence of such an intersection is rare case, because in many cases *Check 2* rejects these intersections. If it happens, we redistribute the centers.

Appendix C: Signed Area and Signed Volume

C1. Signed area of triangle

Figure 12 illustrates an example of an area $S(\sigma_{jk})$ with negative sign. Visually from the figure we obtain the area $S(\sigma_1)$ of concave polygon σ_1 as

$$S(\sigma_1) = -|S(\sigma_{11})| + |S(\sigma_{12})| + |S(\sigma_{13})|. \tag{C.1}$$

If the vertices are sorted in a constant direction, we can calculate it automatically as

$$S(\sigma_1) \equiv |S'(\sigma_1)|, \tag{C.2}$$

where

$$S'(\sigma_1) = S'(\sigma_{11}) + S'(\sigma_{12}) + S'(\sigma_{13}) \tag{C.3}$$

and

$$S'(\sigma_{1k}) = \frac{1}{2}\begin{vmatrix} x_{\lambda k+1} - x_{\lambda 1} & y_{\lambda k+1} - y_{\lambda 1} \\ x_{\lambda k+2} - x_{\lambda 1} & y_{\lambda k+2} - y_{\lambda 1} \end{vmatrix}, \quad k = 1,2,3 \tag{C.4}$$

where the coordinate of vertices λ_{jk} is denoted by $(x_{\lambda k}, y_{\lambda k})$. Therefore, we can calculate the signed area $S(\sigma_{1k});\ k = 1,2,3$ as follows.

$$S(\sigma_{1k}) = \begin{cases} S'(\sigma_{1k}); & S'(\sigma_1) > 0 \\ -S'(\sigma_{1k}); & S'(\sigma_1) < 0 \end{cases} = S'(\sigma_{1k}) \frac{S'(\sigma_1)}{|S'(\sigma_1)|} \tag{C.5}$$

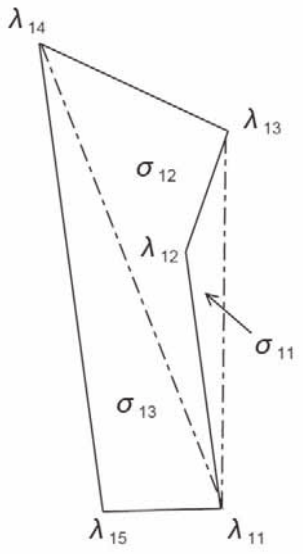

Fig.12. An example of decomposition of base σ_1 into triangles $\sigma_{11}(\lambda_{11},\lambda_{12},\lambda_{12})$, $\sigma_{12}(\lambda_{11},\lambda_{13},\lambda_{14})$, and $\sigma_{13}(\lambda_{11},\lambda_{14},\lambda_{15})$. The area $S(\sigma_{11})$ is negative value, and the other areas $S(\sigma_{12})$ and $S(\sigma_{13})$ are positive values.

C2. Signed Volume of Pyramid

First the signed height $\vec{h}_j$ of pyramid $o_i\sigma_j$ is defined in order to define the signed volume $V(o_i\sigma_j)$. The basic concept of the signed volume is the same as signed area. Figure 13 shows an example of a concave Voronoi polyhedron which has a pyramid $o_i\sigma_j$. The height $\vec{h}_j$ is negative value as shown in Fig.14. Then the volume $V(o_i\sigma_j)$ is negative value. The signed height $\vec{h}_j$ is defined as follows.

$$\vec{h}_j = \begin{cases} |\vec{h}_j| & ;\vec{h}_j\cdot\vec{n}_k > 0 \\ -|\vec{h}_j| & ;\vec{h}_j\cdot\vec{n}_k < 0 \end{cases} = |\vec{h}_j|\frac{\vec{h}_j\cdot\vec{n}_k}{|\vec{h}_j\cdot\vec{n}_k|} \tag{C.6}$$

where $\vec{n}_k$ is the normal vector of the boundary polygon $c_k(\supset\sigma_j)$ and $\vec{h}_j$ is the vector from the o_i to the midpoint between the center o_i and symmetry point m_k.

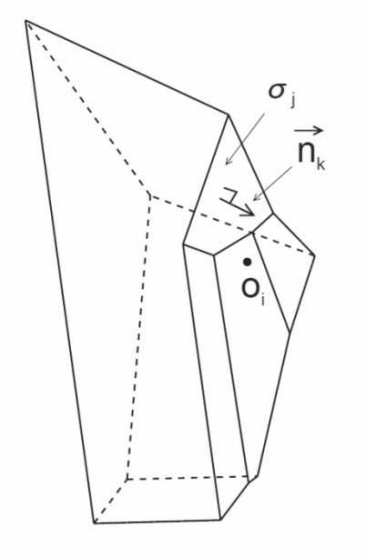

Fig.13. Figure of a concave Voronoi polyhedron which has pyramid $o_i\sigma_j$.

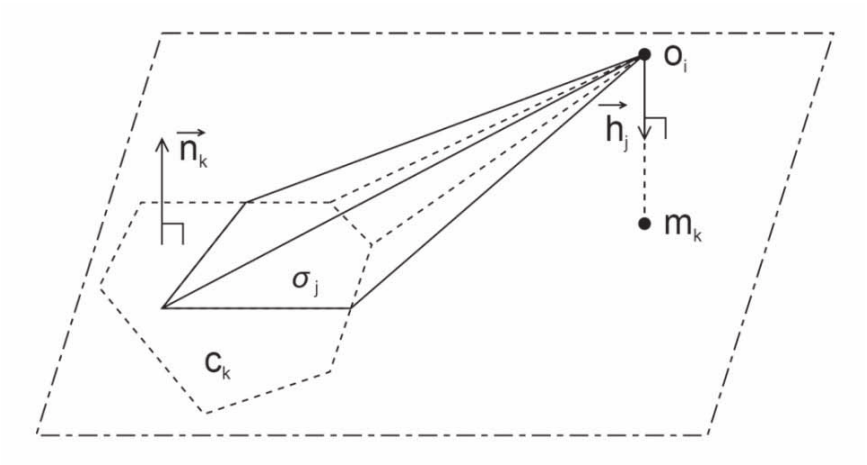

Fig.14. A pyramid $o_i\sigma_j$ of which the sign of volume is negative value.

References

Abramowitz, M. and Stegun,I.A., *Handbook of Mathematical Functions: with Formulas, Graphs, and Mathematical Tables*, Dover Books on Mathematics, 1965.

Ashcroft, N.W. and Mermin, N.D., *Solid State Physics*, Sounders, Philadelphia, 1976.

Averill, F.W. and Painter, G.S., "Pseudospherical integration scheme for electronic-structure calculations", *Phys. Rev. B* vol.39, 1989, pp.8115～8121.

Becke, A.D., "A multicenter numerical integration scheme for polyatomic molecules", *J. Chem. Phys.* vol.88, 1988, pp.2547～2553.

Boerrigter, P.M., Velde, G.te, and Baerends, E.J., "Three-dimensional numerical integration for electronic structure calculations", *J. Int. J. Quantum Chem.* vol.33, 1988, pp.87～113.

Dirac, P.A.M., "Note on exchange phenomena in the Thomas atom", *Proc. Camb. Phil. Soc.* vol.26, 1930, pp.376～395.

Dreizler, R.M. and Gross, E.K.U. *Density Functional Theory*, Springer-Verlag, Berlin, 1990.

Fermi, E., "Un Metodo Statistico per la Determinazione di alcune Prioprieta dell'Atomo" *Rend. Accad. Naz. Lincei*, vol.6, 1927, pp.602～607.

Finney, J.L., "A procedure for the construction of Voronoi polyhedral", *J. Comput. Phys*. vol.32, 1979, pp.137～143.

Huber, K.P. and Herzberg, G., *Molecular Spectra and Molecular structure IV constants of diatomic molecules*, Van Nostrand Reinhold Company Inc., 1979.

Kittel, C., *Introduction to Solid State Physics*, 6th edition, John Wiley & Sons. New York, 1986.

Kryachko, E.S. and Ludena, E.V., *Energy Density Functional Theory of Many-Electron Systems*, Kluwer Academic Publishers, 1990.

Press, W.H., Flannery, B.P., Teukolsky, S.A., and Vetterling, W.T, *Numerical Recipes in Fortran 77: The Art of Scientific Computing*, Cambridge University Press , 1992.

Salvat, F., Martinez, J.D., Mayol, R. and Parellada, J., "Analytical Dirac- Hartree-Fock-Slater screening function for atoms (Z=1–92)", *Phys. Rev. A* vol.36, 1987, pp.467～474.

Slater, J.C., "A Simplification of the Hartree-Fock Method", *Phys. Rev.* vol.81, 1951, pp.385～390.

Stroud, A.H., *Approximate Calculations of Multiple Integrals*, Prentice-Hall, Englewood Cliffs, NJ, 1971.

Szabo, A. and Ostlund, N.S. *Modern Quantum Chemistry*, Macmillan, Tokyo, 1982.

Tanemura, M., Ogawa, T. and Ogita, N., "A new algorithm for three-dimensional voronoi tessellation", *J. Comput. Phys.* vol.51, 1983, pp.191～207.

Thomas, L.H., "The calculation of atomic fields" *Proc. Cambridge Phil. Soc.* vol.23, 1927, pp.542～548.

Velde, G.te and Baerends, E.J., "Numerical integration for polyatomic systems", *J. Comput. Phys.* vol.99, 1992, pp.84～98.

Voronoi, G., "Recherches sur les paralléloèdres Primitives", *J. Reine Angew. Math.* vol.134, 1908, pp.198～287.